Topological responses from gapped Weyl points in 2D altermagnets

Kirill Parshukov,* Raymond Wiedmann,* and Andreas P. Schnyder†
Max Planck Institute for Solid State Research, Heisenbergstrasse 1, D-70569 Stuttgart, Germany
(Dated: March 15, 2024)

Altermagnetism combines aspects of both ferromagnetism and antiferromagnetism, breaking spin degeneracy while possessing no net magnetization. In this work, we study the symmetry requirements for topologically protected Weyl points in 2D altermagnets, involving bands with the same spin quantum number. We classify all spin-wallpaper groups whose symmetries protect 2D Weyl points and show that their nontrivial topology is charactrized by a quantized π-Berry phase. Representative electronic tight-binding and magnonic linear spin-wave models are constructed to investigate the unusual transport characteristics of these 2D Weyl points. Different mass terms, induced for example through strain or via coupling to light or a substrate, gap out the Weyl points leading to emerging gapped topological phases. Depending on the mass terms, these phases carry finite Chern and/or spin Chern numbers and exhibit protected edge states as well as anomalous electronic and thermal Hall responses. We calculate these Hall currents for the different topological phases.

Two-dimensional (2D) materials have attracted much attention since the discovery of graphene, which showcases unique properties in terms of electronic, mechanical, and thermal behavior [1]. Since then, a variety of two-dimensional materials has been studied [2]. Graphene is the prime example of a topological band structure in 2D, as it exhibits protected Dirac points. While Dirac points are linear crossings between spin-degenerate bands, a different type of topological band crossing, Weyl points (WPs), can emerge by splitting the spin degeneracy of the bands, either with strong spin-orbit coupling, an applied magnetic field or by ferro- or ferrimagnetic order. Recently, a variety of 2D ferromagnetic Weyl semimetals has been found, which exhibit fully spin-split band structures [3–5]. In antiferromagnetic materials, where the magnetic order is compensated, the bands are spin degenerate and Weyl crossings are generally not possible. The question, therefore, arises, how WPs in two-dimensional compensated magnetic systems could arise.

In the last few years, there has been an increasing interest in altermagnetic materials both from the theoretical [6–9] and the experimental side [10–14]. Altermagnets exhibit compensated collinear magnetic order, as in antiferromagnets, with spin-split bands, as in ferromagnets. In contrast to antiferromagnets, the magnetic sublattices in altermangets are connected by rotation or mirror symmetries, leading to spin-split bands at a general position which, in particular, does not stem from spin-orbit coupling and can reach comparably large values. The vanishing net magnetization makes these phases robust against magnetic field perturbation, and, therefore, in combination with the possibility of controlling the individual spin channels, promising for spintronic applications [7]. Further, altermagnets in conjunction with superconductivity give rise to a number of interesting phenomena, including unconventional Josephson effects [15, 16], diode effects [17], Cooper-pair splitting [18, 19], and topological superconductivity [20–23].

In this work, we study the symmetries protecting WP degeneracies in 2D altermagnets and provide the symmetry classification for all spin-wallpaper groups compatible with altermagnetic order. We construct an electronic tight-binding and magnon linear spin-wave model for one of the symmetry groups which enable WP degeneracies and discuss the semimetallic bandstructures. We study the phase diagram for different symmetry-breaking mass terms for both models and find a variety of topologically non-trivial phases. For each of the phases, we discuss topological responses in terms of anomalous electronic and thermal conductivity and the spin Hall and spin Nernst effects.

Weyl points protected by altermagnetic symmetries.— Altermagnets are a novel phase with negligible spin-orbit coupling and compensated collinear magnetic order. Its symmetries are described by spin-space groups [24–31], for which actions on lattice and spin degrees of freedom are decoupled. A group element $(s||g)$ represents the action s on spin and g on the lattice. The collinear spin arrangement along the z axis allows for the SO(2) spin rotation, and the group actions $\mathbb{Z}_2^T = (E||E) + (2_x\mathcal{T}||E)$. The element $(2_x\mathcal{T}||E)$ flips the spin twice with the 2-fold spin rotation 2_x and time-reversal operator $\mathcal{T}$ that also acts on the lattice degrees of freedom. The total magnetic moment is compensated due to a symmetry that acts non-trivially on spin and lattice, such as the mirror symmetry $(2_x||M)$. The mirror and SO(2) spin-rotational symmetries enforce a line degeneracy along the mirror line between bands with opposite spins. However, an energy splitting between bands with opposite spins is allowed at a general position (GP) in the Brillouin zone (BZ). The states are non-degenerate and have well-defined spin at a GP. If two bands with the same spin come close to each other, they can form a WP crossing. In two-dimensional systems, this point degeneracy must be protected by symmetries. Generally, space-time inversion $2_z\mathcal{T}$ and mirror symmetries quantize the Berry phase protecting WPs [32]. These symmetries exist in

* These two authors contributed equally.
† a.schnyder@fkf.mpg.de

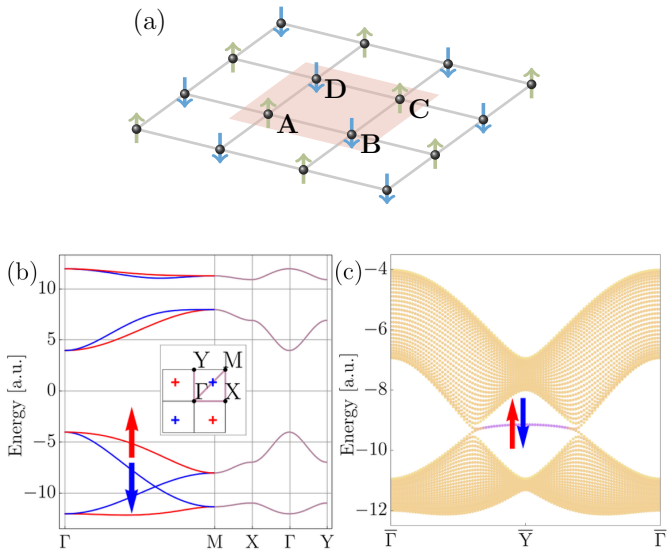

Figure 1: (a) Altermagnetic lattice with collinear magnetic order and four sites per unit cell (red area). (b) Electronic bands of the altermagnetic tight-binding Hamiltonian (1) with spin quantum number indicated by the arrows and red/blue color. The inset shows the location of the four WPs in the 2D BZ. (c) Edge band structure of the electronic states within the 10 outermost unit cells of a 30 layers ribbon.

altermagnets, however, they must not act on the spin to avoid enforced spin degeneracies. In altermagnets with $(2_x\mathcal{T}||2_z)$(or $(E||M)$), we expect to observe protected WP degeneracies at GPs (or on mirror lines) between bands with the same spin. The spin polarization of the 2D WPs in altermagnets allows for an interesting interplay between spin currents, topology, and magnetism.

In Tab. I we list all altermagnetic spin-wallpaper groups that can protect the Weyl crossings. Group elements that flip the spin are denoted with $\bar{1}$. Information on the enumeration can be found in the Supplemental Material (SM) [33]. The number of the WPs is always a multiple of four due to symmetries that relate the point crossings. In the remainder of this paper, we consider the altermagnetic wallpaper group $\mathrm{p}^{\bar{1}}4^{\bar{1}}\mathrm{m}^1\mathrm{m}$. The lattice with a four-site unit cell is shown in Fig. 1. Mirror symmetries $(2_x||m_x), (2_x||m_y)$ relate sublattices with opposite magnetic moments, i.e., under these operations site A is mapped to sites B and C, respectively. The mirrors enforce spin degeneracies along $k_x, k_y = 0, \pi$ lines. The spin degeneracy is lifted at GPs allowing for spin-polarized WPs protected by the $(2_x\mathcal{T}||2_z)$ symmetry.

Electronic model.— First, we consider the electronic tight-binding model with symmetries of the altermagnetic wallpaper group $\mathrm{p}^{\bar{1}}4^{\bar{1}}\mathrm{m}^1\mathrm{m}$ (for the symmetry representations see SM [33]). The Wyckoff positions $(\frac{1}{4},\frac{1}{4},m_z)$, $(\frac{3}{4},\frac{1}{4},\overline{m_z})$, $(\frac{3}{4},\frac{3}{4},m_z)$ and $(\frac{1}{4},\frac{3}{4},\overline{m_z})$ correspond to the sites A, B, C and D. The alignment of the magnetic moments is along the z axis, so that at A, C (B, D) sites they point in the same direction. A symmetric model in k-space is given by

WP, $(2_x T\|\|2_z)$	$\mathrm{p}^1\mathrm{2}^{\bar{1}}\mathrm{m}^{\bar{1}}\mathrm{m}$, $\mathrm{p}^1\mathrm{2}^{\bar{1}}\mathrm{m}^{\bar{1}}\mathrm{g}$, $\mathrm{p}^1\mathrm{2}^{\bar{1}}\mathrm{g}^{\bar{1}}\mathrm{g}$, $\mathrm{c}^1\mathrm{2}^{\bar{1}}\mathrm{m}^{\bar{1}}\mathrm{m}$, $\mathrm{p}^{\bar{1}}\mathrm{4}$, $\mathrm{p}^{\bar{1}}4^{\bar{1}}\mathrm{m}^1\mathrm{m}$, $\mathrm{p}^{\bar{1}}4^1\mathrm{m}^{\bar{1}}\mathrm{m}$, $\mathrm{p}^1 4^{\bar{1}}\mathrm{m}^{\bar{1}}\mathrm{m}$, $\mathrm{p}^{\bar{1}}4^{\bar{1}}\mathrm{g}^1\mathrm{m}$, $\mathrm{p}^{\bar{1}}4^1\mathrm{g}^{\bar{1}}\mathrm{m}$, $\mathrm{p}^1 4^{\bar{1}}\mathrm{g}^{\bar{1}}\mathrm{m}$, $\mathrm{p}^1 6^{\bar{1}}\mathrm{m}^{\bar{1}}\mathrm{m}$,
WP, $(E\|\|M)$	$\mathrm{p}^{\bar{1}}4^{\bar{1}}\mathrm{m}^1\mathrm{m}$, $\mathrm{p}^{\bar{1}}4^1\mathrm{m}^{\bar{1}}\mathrm{m}$, $\mathrm{p}^{\bar{1}}4^{\bar{1}}\mathrm{g}^1\mathrm{m}$, $\mathrm{p}^{\bar{1}}4^1\mathrm{g}^{\bar{1}}\mathrm{m}$

Table I: Altermagnetic spin-wallpaper groups that protect WPs between bands with the same spin.

$$H(\mathbf{k}) = \begin{pmatrix} H_\downarrow(\mathbf{k}) + N\Sigma_z & 0 \\ 0 & H_\downarrow(\mathbf{k}) - N\Sigma_z \end{pmatrix}, \tag{1a}$$

$$H_\downarrow(\mathbf{k}) = \begin{pmatrix} \epsilon & t_{\mathrm{AB}} & t_{\mathrm{AC}} & t_{\mathrm{AD}} \\ t^*_{\mathrm{AB}} & \epsilon & t_{\mathrm{BC}} & t_{\mathrm{BD}} \\ t^*_{\mathrm{AC}} & t^*_{\mathrm{BC}} & \epsilon & t_{\mathrm{CD}} \\ t^*_{\mathrm{AD}} & t^*_{\mathrm{BD}} & t^*_{\mathrm{CD}} & \epsilon \end{pmatrix}, \tag{1b}$$

where we take $\epsilon = 0$, $t_{\mathrm{AB}} = -t_{\mathrm{CD}} = 4i\sin\frac{k_x}{2}$, $t_{\mathrm{AC}} = 2(\cos\frac{k_x-k_y}{2} + \cos\frac{k_x+k_y}{2} - i\sin\frac{k_x+k_y}{2})$, $t_{\mathrm{AD}} = t_{\mathrm{BC}} = 4i\sin\frac{k_y}{2}$, $t_{\mathrm{BD}} = 2(\cos\frac{k_x-k_y}{2} + \cos\frac{k_x+k_y}{2} + i\sin\frac{k_x-k_y}{2})$, $N = 8$. Matrix $\Sigma_z = \mathrm{diag}(1,-1,1,-1)$ describes an interaction with the staggered magnetic moments. The band structure shown in Fig. 1(b) has enforced line spin degeneracies along the k_x, k_y mirror lines and the bands are spin split at GPs. Four spin-polarized WPs emerge along the ΓM lines and are related by the symmetries of the model (Fig. 1). Every crossing carries a π-Berry phase and has a spin flavor. These two facts make the semimetallic phase intriguing. A non-trivial Berry phase along a path through the whole BZ indicates, by the bulk-boundary correspondence, the emergence of edge states [32, 34]. As the Hilbert space contains two decoupled subspaces with well-defined spin, the Berry phase and bulk-boundary correspondence can be introduced for them separately. Two boundary states with opposite spin emerge at each of the two edges (see Fig. 1).

In a system with the chemical potential near the degeneracy, the low-energy physics is governed by the four spin-polarized WPs. Under the $(2_x\mathcal{T}||2_z)$ symmetry breaking we expect an anomalous spin-polarized current from each of the four valleys. Depending on the mass term the currents can compensate or enhance each other leading to a rich phase diagram. To study the variety of the phases we construct the low-energy model for each of the crossings. The construction procedure and the low-energy models for all four WPs/valleys can be found in the SM [33]. Each of the models can be described by the effective Hamiltonian

$$H^{\mathrm{eff}}_\alpha(\mathbf{q}) = \epsilon_\alpha(\mathbf{q})\sigma_0 + \sum_{i,j\in\{x,y\}} q_i(\mathcal{A}_\alpha)_{ij}\sigma_j, \tag{2}$$

where the WP in each of the four quarters of the BZ is labelled by $\alpha \in \{\pm\pm, \pm\mp\}$, $\mathbf{q}$ is the displacement from the WP, σ_i are the Pauli matrices, and the matrix $\mathcal{A}_\alpha$

contains the velocities. The symmetries of the spin-space group relate the four matrices $\mathcal{A}_\alpha$ with each other. The term $\epsilon_\alpha(\mathbf{q})\sigma_0$ is not essential for the topological properties, but relevant for our calculations of the conductivity.

To gap out the WPs we break the $(2_x\mathcal{T}||2_z)$, $(E||m_{xy})$ and $(E||m_{x\overline{y}})$ symmetries. Since these symmetries relate sublattice A with C (B with D), we introduce mass terms in the form of staggered potentials and hoppings

$$M(\mathbf{k}) = m(\mathbf{k})\ \mathrm{diag}(+1,+1,-1,-1), \tag{3}$$

where $m(\mathbf{k})$ is positive for the A, B sublattices and negative for the C, D sublattices. In particular, we consider a phase diagram for the three masses $m(\mathbf{k}) = m_1 + m_2\sin(k_x) + m_3\sin(k_y)$. These mass terms do not mix spin up and down allowing for spin-polarized valleys. The onsite term m_1 can be implemented using a staggered sublattice potential [35] that breaks inversion $(E||2_z)$, whereas the k-dependent terms also break time-reversal $(2_x\mathcal{T}||E)$ symmetry. Functionally similar terms can be realized in a quasistatic system with laser driving (see Ref. [36] and SM [33]), where light intensity is a tuning parameter between distinct phases.

The low-energy effective mass term that opens a gap in Eq. (2) lifting the point degeneracy has the form $m_\alpha\sigma_z$. Each valley contributes to the total (spin) Chern number of the split bands as

$$C^\alpha = \pm\tfrac{\mathrm{sign}(m_\alpha \det \mathcal{A}_\alpha)}{2}. \tag{4}$$

We compute the phase diagram by calculating the Chern number and spin Chern number $C_S = C_\downarrow - C_\uparrow$ contribution from each of the crossings and summing them up (see Fig. 2). For distinct phases, we show the Berry curvature distribution. Non-zero values of the (spin) Chern number imply the presence of topological boundary states for a model with edges. We compute the edge band structure for ribbons with termination in the x-direction and 30 layers. In Fig. 2 we display a projection of the bands onto 10 unitcells at the left edge. In addition, we show the spin character for the emerging edge states. In the phase with the bulk Chern number $C = 2$, $C_S = 0$ we observe two boundary states with opposite spins and positive Fermi velocity for the chemical potential in the gap. When $C = 0$, $C_S = 2$ the states are spin-polarized and have opposite Fermi velocities. In the phase with $C = 1$, $C_S = -1$ there is a spin-up polarized edge state with positive Fermi velocity inside the bulk gap.

Electronic transport — The model shows topological response, as the non-trivial Chern number corresponds to the quantized transversed current. In the semiclassical limit the Hall current has the form [37, 38]

$$\mathbf{j} = \frac{e^2}{\hbar}\int \frac{d^2\mathbf{k}}{(2\pi)^2} f(\mathbf{k})\mathbf{E}\times\Omega(\mathbf{k}), \tag{5}$$

where $f(\mathbf{k})$ is the Fermi-Dirac distribution, $\mathbf{E}$ is the electric field, $\Omega(\mathbf{k})$ is the Berry curvature. We choose the chemical potential μ within the conduction band, above the gap energy $|m|$, i.e. $|m| < E_+ < \mu$. The total current contains contributions from four Fermi pockets, described by the spin-polarized low-energy models. Integrating the expression for each of the valleys in the limit of small gap $|m| \ll \mu$ and temperature $T = 0$, we obtained an analytical expression for the transverse (spin) conductivity

$$\sigma_{xy} = \frac{e^2}{2h}\sum_\alpha \mathrm{sign}(m_\alpha \det \mathcal{A}_\alpha) + O(m_\alpha/\mu), \tag{6}$$

$$\sigma^S_{xy} = \frac{e}{8\pi}\sum_\alpha (-1)^{s(\alpha)}\mathrm{sign}(m_\alpha \det \mathcal{A}_\alpha) + O(m_\alpha/\mu), \tag{7}$$

where we also consider the spin current $\mathbf{j}^S = (\hbar/2e)(\mathbf{j}_\downarrow - \mathbf{j}_\uparrow)$. Here, $s(\alpha) = 0$ for the crossings α with spin down, and $s(\alpha) = 1$ otherwise. The main contribution to the conductivity is due to the quantized anomalous current if the gap is small $|m| \ll \mu$. For the case when the chemical potential is inside the gap, we computed the temperature dependence of the (spin) transverse conductivity using Eq. (5). In the non-trivial phases, the conductivity reaches quantized values for small temperatures (Fig. 2).

Magnon model.— Analogously to the electronic model introduced in the previous section, we study the magnon band structure of a minimal model for altermagnetic wallpaper group $\mathrm{p}^{\overline{1}}4^{\overline{1}}\mathrm{m}^1\mathrm{m}$ for the lattice shown in Fig. 1. The four sites in the unit cell result in four magnon bands which inherit the altermagnetic spin-space symmetries of the exchange interactions, in particular including the $(2_x\mathcal{T}||2_z)$ symmetry which can protect WPs. The spin interaction Hamiltonian for the localized magnetic moments reads

$$\mathcal{H} = J\sum_{\langle ij\rangle}\mathbf{S}_i\mathbf{S}_j + L^{(\prime/\prime\prime)}\sum_{\langle\langle ij\rangle\rangle}\mathbf{S}_i\mathbf{S}_j \tag{8}$$

with J the nearest-neighbor coupling strength between opposite-spin sublattices and $L^{(\prime/\prime\prime)}$ the next-nearest-neighbor coupling strengths between same-spin sublattices. The couplings are shown in the lattice structure in the SM [33]. Performing the standard linear spin-wave theory we obtain the magnon Hamiltonian in momentum space $\mathcal{H} = \sum_{\mathbf{k}}\psi^\dagger_{\mathbf{k}}H_{\mathbf{k}}\psi_{\mathbf{k}}$ in terms of the bosonic operators $\psi_{\mathbf{k}} = (a_{\mathbf{k}}, b^\dagger_{-\mathbf{k}}, c_{\mathbf{k}}, d^\dagger_{-\mathbf{k}})^{\mathrm{T}}$ with

$$H_{\mathbf{k}} = S\begin{pmatrix} h_0 & \gamma_1 & \gamma_2 & \gamma_3 \\ \gamma_1 & h_0 & \gamma_3 & \gamma_4 \\ \gamma_2^* & \gamma_3^* & h_0 & \gamma_1 \\ \gamma_3^* & \gamma_4^* & \gamma_1 & h_0 \end{pmatrix} \tag{9}$$

where $h_0 = 4J - 2L - L' - L''$, $\gamma_1 = 2J\cos\frac{k_x}{2}$, $\gamma_2 = 2L\cos\frac{-k_x+k_y}{2} + L'e^{i\frac{k_x+k_y}{2}} + L''e^{-i\frac{k_x+k_y}{2}}$, $\gamma_3 = 2J\cos\frac{k_y}{2}$, and $\gamma_4 = 2L\cos\frac{k_x+k_y}{2} + L'e^{i\frac{-k_x+k_y}{2}} + L''e^{i\frac{k_x-k_y}{2}}$. The Hamiltonian is diagonalized with a Bogoliubov transformation and the resulting magnon spectrum is shown in Fig. 3(a). One finds that the magnon bands are pairwise degenerate along the high-symmetry path $\mathrm{M}-\mathrm{X}-\Gamma-\mathrm{Y}$,

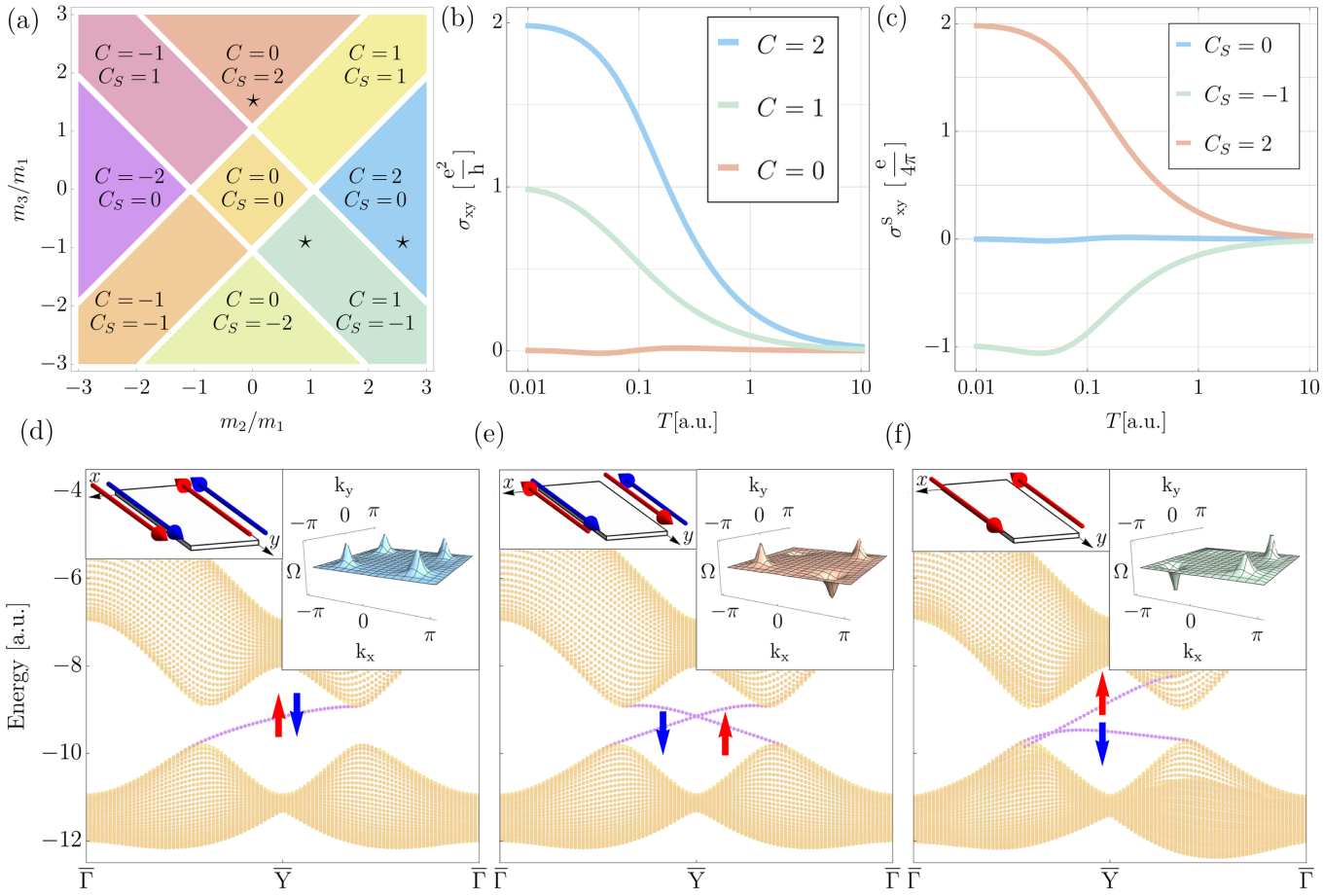

Figure 2: (a) Altermagnet phase diagram as a function of the mass terms $m(\mathbf{k}) = m_1 + m_2 \sin k_x + m_3 \sin k_y$ (with $m_1 > 0$), which gap out the 2D WPs. (b), (c) Transverse charge and spin conductivity, respectively, of Hamiltonian (1) as a function of temperature T with the chemical potential inside the gap. (d)-(f) Edge band structure of the states within the ten outermost unit cells of a ribbon with mass terms (3) for the phase with $C = 2$, $m_1 = m_3 = 0$, $m_2 = 0.5$. (e) Quantum spin Hall state with $C_S = 2$, $m_1 = m_2 = 0$, $m_3 = 0.5$. (f) Quantum Hall state with spin-polarized current $C = 1$, $C_S = -1$, $m_1 = 0.4$, $m_2 = 0.5$, $m_3 = -0.5$.

but are in general split in the rest of the BZ. A distinct chirality, corresponding to the direction of precession of the spin around the axis of the collinear magnetic order, can be assigned to the individual magnon bands. Since the collinear order in z-direction preserves the z-component of the total spin $S^z = \sum_{i,\delta} S^z_{i,\delta}$ with δ running over the sublattices, we use $\vartheta = \langle S^z \rangle / \hbar$ to specify the chirality of the bands. In particular, we have $\vartheta = +1$ for right-handed and $\vartheta = -1$ for left-handed magnon modes and we indicate them with curved arrows ↻ and ↺, respectively. In antiferromagnetic systems, bands of opposite chirality are generally degenerate over the entire BZ, due to inversion or fractional translation symmetries connecting the opposite-spin sublattices. In altermagnetic systems, however, these symmetries are broken, which manifests in chirality-split bandstructures. The remaining degeneracies along high-symmetry paths in our model are enforced by mirror symmetries relating opposite-spin sublattices. As for the electronic bands, the magnon bands exhibit four WPs formed by same-chirality bands, which are protected by the $(2_x\mathcal{T}||2_z)$ symmetry. A four-fold rotational symmetry relates the positions of the crossings and pins them to the ΓM line. For each of the crossings we find a finite quantized Berry phase of π. Calculating the magnon spectrum for a ribbon of finite width in y-direction, we find edge states between the projected WPs. In the spectrum shown in Fig. 3(b), the bands are projected onto the lower edge. The topological edge states, which arise between the projections of the WPs are highlighted in pink. Even though the topologically protected edge states are not energetically distinguishable from the projected bulk states, they can be identified due to their exponential localization at the boundary. We find in total two degenerate bands of opposite chirality per edge.

Next, we study the properties of the gapped system obtained by considering the mass term introduced in Eq. (3) with $m(\mathbf{k}) = m_1 + m_2 \sin(k_x) + m_3 \sin(k_y)$,

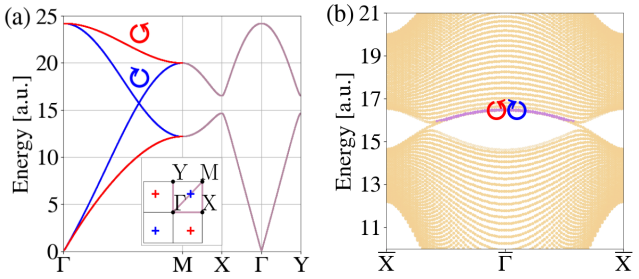

Figure 3: (a) Magnon bulk band structure of the Hamiltonian (9) along high-symmetry path for the parameters $J = 2$, $L = -3$, $L' = L/2$, $L'' = L/5$. The chirality of the magnons is indicated with curved arrows and red (blue) coloured bands for right- (left-)handed chirality. The inset shows the BZ with the high-symmetry points and the crosses mark the positions of the WPs and their chirality. (b) Magnon edge spectrum on a ribbon geometry with 50 unit cells in y-direction projected onto ten unit cells at the lower boundary of the ribbon for the same parameters as in (a). The chirality-degenerate topological edge state is marked in pink.

as discussed for the electron model, which breaks the $(2_x\mathcal{T}||2_z)$, $(E||m_{xy})$ and $(E||m_{x\bar{y}})$ symmetries, thereby splitting the WPs. While in the electronic system, a low-energy model is constructed to study the effect of the mass term and the resulting phases, for the magnon system, we continue to consider the full spectrum. We obtain the phase diagram for the ratio of the mass parameters m_2/m_1 and m_3/m_1 by calculating the Chern number C of the lower two bands as an integral of the non-Abelian Berry curvature. Further, we calculate the magnon analog of the spin Chern number, the chirality Chern number $C_\vartheta = C_{+1} - C_{-1}$ with $C_{\pm 1}$ the Chern number for the bands with chirality ± 1. The phase diagram we obtain is in full agreement with the one determined for the low-energy electron model shown in Fig. 2 with $C_\vartheta = C_S$. Details on the calculation and the resulting phase diagram for the magnon model are described in the SM [33]. In the topological phases, i.e., phases with finite (chirality) Chern number, we calculate the edge spectra on a ribbon of finite width in y-direction and show the projection onto the lower edge in Fig. 4. The topological edge states with their respective magnon chirality are highlighted in pink. As in the electron model, for each edge we find two degenerate edge states of opposite chirality in the phase with $C = 2$ and $C_\vartheta = 0$ [Fig. 4(a)], two counter-propagating edge states with opposite chirality for $C = 0$ and $C_\vartheta = 2$ [Fig. 4(b)], and one edge state with chirality $+1$ for $C = 1$ and $C_\vartheta = 1$ [Fig. 4(c)].

Thermal response.— The non-trivial topology of gapped magnon bands can be studied experimentally via thermal transport measurements. In the semiclassical limit, in systems with a gap with $C \neq 0$, the finite Berry curvature leads to a thermal Hall current $\mathbf{j} = \kappa^{xy}\hat{z} \times \nabla T$ when applying a longitudinal thermal gradient. In the case of $C_\vartheta \neq 0$, one finds the magnon spin Nernst effect with the chirality current $\mathbf{j} = \alpha^{xy}\hat{z} \times \nabla T$ as the analogue of the spin Hall effect in electronic systems. The thermal Hall conductivity $\kappa^{xy}(T)$ [39] and the magnon spin Nerst coefficient $\alpha^{xy}(T)$ [40] for a 2D magnon system are given by

$$\kappa^{xy}(T) = -\frac{k_B^2 T}{(2\pi)^2\hbar} \sum_n \int_{BZ} \mathrm{d}^2k \, c_2(\varrho_n)\, \Omega_n(\mathbf{k}), \tag{10}$$

$$\alpha^{xy}(T) = -\frac{k_B}{(2\pi)^2\hbar} \sum_n \int_{BZ} \mathrm{d}^2k \, c_1(\varrho_n)\, \vartheta_n \Omega_n(\mathbf{k}), \tag{11}$$

where $\varrho_i = [e^{\varepsilon_n(\mathbf{k})/(k_B T)} - 1]^{-1}$ is the bosonic distribution function for energy band $\varepsilon_n(\mathbf{k})$, $\Omega_n(\mathbf{k})$ is the Berry curvature of band n, ϑ_n its chirality, $c_1(x) = (1+x)\ln(1+x) - x\ln x$, $c_2(x) = (1+x)(\ln\frac{1+x}{x})^2 - (\ln x)^2 - 2\mathrm{Li}_2(-x)$, and $\mathrm{Li}_2(x)$ is the dilogarithm. The insets in Fig. 4 show the thermal Hall conductivity and the magnon spin Nernst coefficient as a function of temperature for the different topological phases. We find a finite thermal Hall effect in the phases with $C \neq 0$ and a finite magnon spin Nernst effect in the phases with $C_\vartheta \neq 0$. In the topologically trivial phase, both responses are zero. Since magnons are bosons, the response is not quantized and the strength of the response depends on the parameters of the model and the mass term.

Conclusion.— In this work, we studied degeneracies between bands with the same spin quantum number in 2D altermagnets. These intriguing types of degeneracies have recently been theoretically investigated in a 2D variant of the Lieb lattice [41], where they are protected by mirror symmetries. We systematically extend the study on these novel features by providing a classification of the degeneracies based on the symmetries for the spin-wallpaper groups. While previous studies focused on electronic systems, we show that these features can also arise in magnon systems by constructing both, an electron tight-binding and a magnon model for the spin-wallpaper group $\mathrm{p}\bar{1}4\bar{1}\mathrm{m}1\mathrm{m}$, which both, indeed, exhibit four symmetry-related WPs involving bands of opposite spin/chirality. Each WP has a well-defined spin (chirality) quantum number and exhibits a parity anomaly [42, 43] leading to topological currents (see SM [33]). Spin(chirality) polarization of the electronic(magnonic) states in the vicinity of the WPs together with the absence of the total magnetization of the altermagnet allows for unique topological responses. Under a $(2_x\mathcal{T}||2_z)$-breaking mass term we study the phase diagram which contains a variety of topological phases, giving rise to the quantum Hall and quantum spin Hall effect for electrons, and the thermal Hall and spin Nernst effect for magnons. The time-reversal breaking mass terms can be controlled, for example, by light interacting with the electrons(magnons), allowing to drive the 2D altermagnet across different topological phase transitions (see SM [33]). In the trivial phases, the valley Hall effect [37] is expected due to the selective coupling of the valley electrons to the circularly polarized light. Right

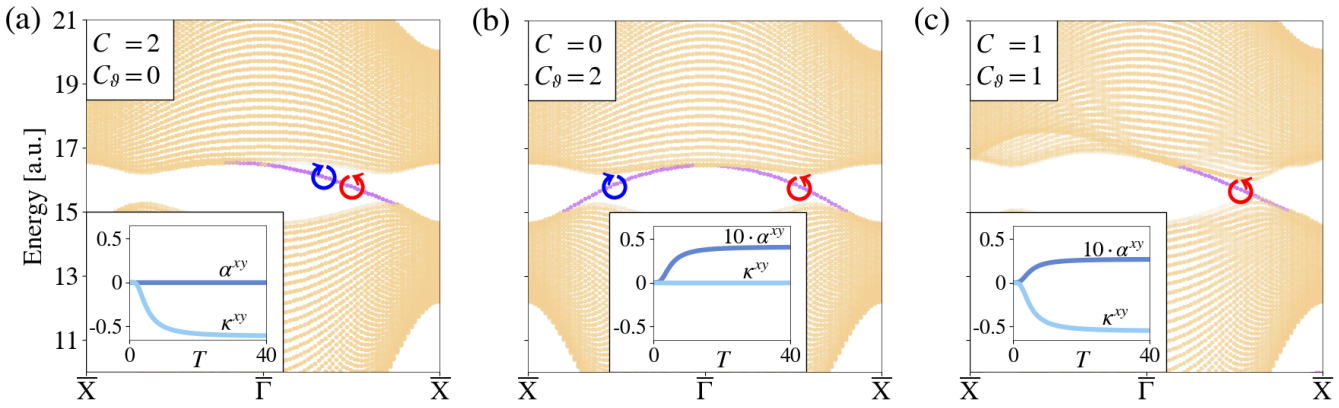

Figure 4: Magnon edge spectra calculated on a ribbon geometry with 50 unit cells in y-direction for different mass terms for the parameters $J = 2$, $L = -3$, $L' = L/2$, $L'' = L/5$. The bands are projected onto ten unit cells at the lower boundary of the ribbon. The topological edge states with their respective magnon chirality are shown in pink. The insets show the transverse thermal conductivity κ^{xy} in units $[k_B^2/\hbar]$ and the magnon spin Nernst coefficient α^{xy} in units $[k_B/\hbar]$ as a function of temperature T for the respective phases. We consider phases with (a) $C = 2$, $C_\vartheta = 0$ with mass parameters $m_2 = 0.5$, $m_1 = m_3 = 0$, (b) $C = 0$, $C_\vartheta = 2$ with mass parameters $m_3 = 0.5$, $m_1 = m_2 = 0$, and (c) $C = 1$, $C_\vartheta = 1$ with mass parameters $m_1 = -0.5$, $m_2 = 0.8$, $m_3 = 0.5$.

and left polarized light couples to electrons from valleys with opposite Chern number contribution. Similarly, the magnon valley thermal Hall effect is expected to arise in the trivial phases of the magnon model, which is, for example, studied for triangular-lattice antiferromagnets in Ref. [44].

Acknowledgments.— We wish to thank Moritz Hirschmann, Niclas Heinsdorf, and Paul McClarty for useful discussions. This work is funded by the Deutsche Forschungsgemeinschaft (DFG, German Research Foundation) – TRR 360 – 492547816.

[1] A. K. Geim, Science **324**, 1530 (2009).
[2] P. Miró, M. Audiffred, and T. Heine, Chemical Society reviews **43 18**, 6537 (2014).
[3] C. Niu, J.-P. Hanke, P. M. Buhl, H. Zhang, L. Plucinski, D. Wortmann, S. Blügel, G. Bihlmayer, and Y. Mokrousov, Nature Communications **10** (2019), 10.1038/s41467-019-10930-6.
[4] S. Jeon, Y.-T. Oh, and Y. Kim, Phys. Rev. B **100**, 035406 (2019).
[5] S. Liu, C. Wang, L. Liu, J.-H. Choi, H.-J. Kim, Y. Jia, C. H. Park, and J.-H. Cho, Phys. Rev. Lett. **125**, 187203 (2020).
[6] L. Šmejkal, J. Sinova, and T. Jungwirth, Phys. Rev. X **12**, 031042 (2022).
[7] L. Šmejkal, J. Sinova, and T. Jungwirth, Phys. Rev. X **12**, 040501 (2022).
[8] L. Šmejkal, A. H. MacDonald, J. Sinova, S. Nakatsuji, and T. Jungwirth, Nature Reviews Materials **7**, 482 (2022).
[9] I. Mazin (The PRX Editors), Phys. Rev. X **12**, 040002 (2022).
[10] Y.-P. Zhu, X. Chen, X.-R. Liu, Y. Liu, P. Liu, H. Zha, G. Qu, C. Hong, J. Li, Z. Jiang, X.-M. Ma, Y.-J. Hao, M.-Y. Zhu, W. Liu, M. Zeng, S. Jayaram, M. Lenger, J. Ding, S. Mo, K. Tanaka, M. Arita, Z. Liu, M. Ye, D. Shen, J. Wrachtrup, Y. Huang, R.-H. He, S. Qiao, Q. Liu, and C. Liu, Nature **626**, 523 (2024).
[11] J. Krempaský, L. Šmejkal, S. W. D'Souza, M. Hajlaoui, G. Springholz, K. Uhlířová, F. Alarab, P. C. Constantinou, V. Strocov, D. Usanov, W. R. Pudelko, R. González-Hernández, A. Birk Hellenes, Z. Jansa, H. Reichlová, Z. Šobáň, R. D. Gonzalez Betancourt, P. Wadley, J. Sinova, D. Kriegner, J. Minár, J. H. Dil, and T. Jungwirth, Nature **626**, 517 (2024).
[12] O. Fedchenko, J. Minár, A. Akashdeep, S. W. D'Souza, D. Vasilyev, O. Tkach, L. Odenbreit, Q. Nguyen, D. Kutnyakhov, N. Wind, L. Wenthaus, M. Scholz, K. Rossnagel, M. Hoesch, M. Aeschlimann, B. Stadtmüller, M. Kläui, G. Schönhense, T. Jungwirth, A. B. Hellenes, G. Jakob, L. Šmejkal, J. Sinova, and H.-J. Elmers, Science Advances **10**, eadj4883 (2024).
[13] J. Nag, B. Das, S. Bhowal, Y. Nishioka, B. Bandyopadhyay, S. Kumar, K. Kuroda, A. Kimura, K. G. Suresh, and A. Alam, "Gdalsi: An antiferromagnetic topological weyl semimetal with non-relativistic spin splitting," (2023), arXiv:2312.11980 [cond-mat.str-el].
[14] Z. Lin, D. Chen, W. Lu, X. Liang, S. Feng, K. Yamagami, J. Osiecki, M. Leandersson, B. Thiagarajan, J. Liu, C. Felser, and J. Ma, "Observation of giant spin splitting and d-wave spin texture in room temperature altermagnet ruo2," (2024), arXiv:2402.04995 [cond-mat.mtrl-sci].
[15] J. A. Ouassou, A. Brataas, and J. Linder, Phys. Rev. Lett. **131**, 076003 (2023).
[16] C. W. J. Beenakker and T. Vakhtel, Phys. Rev. B **108**, 075425 (2023).

[17] S. Banerjee and M. S. Scheurer, "Altermagnetic superconducting diode effect," (2024), arXiv:2402.14071 [cond-mat.supr-con].

[18] H. G. Giil, B. Brekke, J. Linder, and A. Brataas, "Quasiclassical theory of superconducting spin-splitter effects and spin-filtering via altermagnets," (2024), arXiv:2403.04851 [cond-mat.supr-con].

[19] Y. Nagae, A. P. Schnyder, and S. Ikegaya, "Spin-polarized specular andreev reflections in altermagnets," (2024), arXiv:2403.07117 [cond-mat.supr-con].

[20] D. Chakraborty and A. M. Black-Schaffer, "Zero-field finite-momentum and field-induced superconductivity in altermagnets," (2023), arXiv:2309.14427 [cond-mat.supr-con].

[21] B. Brekke, A. Brataas, and A. Sudbø, Phys. Rev. B **108**, 224421 (2023).

[22] S. A. A. Ghorashi, T. L. Hughes, and J. Cano, "Altermagnetic routes to majorana modes in zero net magnetization," (2023), arXiv:2306.09413 [cond-mat.mes-hall].

[23] Y.-X. Li and C.-C. Liu, Phys. Rev. B **108**, 205410 (2023).

[24] A. Kitz, physica status solidi (b) **10**, 455 (1965).

[25] W. F. Brinkman, R. J. Elliott, and R. E. Peierls, Proceedings of the Royal Society of London. Series A. Mathematical and Physical Sciences **294**, 343 (1966).

[26] W. Brinkman and R. J. Elliott, Journal of Applied Physics **37**, 1457 (1966).

[27] D. Litvin and W. Opechowski, Physica **76**, 538 (1974).

[28] Z. Xiao, J. Zhao, Y. Li, R. Shindou, and Z.-D. Song, "Spin space groups: Full classification and applications," (2023), arXiv:2307.10364 [cond-mat.mes-hall].

[29] J. Ren, X. Chen, Y. Zhu, Y. Yu, A. Zhang, J. Li, Y. Liu, C. Li, and Q. Liu, "Enumeration and representation of spin space groups," (2023), arXiv:2307.10369 [cond-mat.mtrl-sci].

[30] Y. Jiang, Z. Song, T. Zhu, Z. Fang, H. Weng, Z.-X. Liu, J. Yang, and C. Fang, "Enumeration of spin-space groups: Towards a complete description of symmetries of magnetic orders," (2023), arXiv:2307.10371 [cond-mat.mtrl-sci].

[31] X. Chen, J. Ren, J. Li, Y. Liu, and Q. Liu, "Spin space group theory and unconventional magnons in collinear magnets," (2023), arXiv:2307.12366 [cond-mat.mtrl-sci].

[32] C. K. Chiu, Y. H. Chan, and A. P. Schnyder, "Quantized berry phase and surface states under reflection symmetry or space-time inversion symmetry," (2018), arXiv:1810.04094 [cond-mat.mes-hall].

[33] See the Supplemental Material at http:... for details on the symmetry classifications, the model descriptions, etc..

[34] J.-W. Rhim, J. Behrends, and J. H. Bardarson, Phys. Rev. B **95**, 035421 (2017).

[35] B. Hunt, J. D. Sanchez-Yamagishi, A. F. Young, M. Yankowitz, B. J. LeRoy, K. Watanabe, T. Taniguchi, P. Moon, M. Koshino, P. Jarillo-Herrero, and R. C. Ashoori, Science **340**, 1427 (2013).

[36] T. Oka and H. Aoki, Phys. Rev. B **79**, 081406 (2009).

[37] D. Xiao, W. Yao, and Q. Niu, Phys. Rev. Lett. **99**, 236809 (2007).

[38] D. Xiao, M.-C. Chang, and Q. Niu, Rev. Mod. Phys. **82**, 1959 (2010).

[39] R. Matsumoto and S. Murakami, Phys. Rev. Lett. **106**, 197202 (2011).

[40] R. Cheng, S. Okamoto, and D. Xiao, Phys. Rev. Lett. **117**, 217202 (2016).

[41] D. S. Antonenko, R. M. Fernandes, and J. W. F. Venderbos, "Mirror chern bands and weyl nodal loops in altermagnets," (2024), arXiv:2402.10201 [cond-mat.mes-hall].

[42] A. J. Niemi and G. W. Semenoff, Phys. Rev. Lett. **51**, 2077 (1983).

[43] W. B. Rui, Y. X. Zhao, and A. P. Schnyder, Phys. Rev. B **97**, 161113 (2018).

[44] Q.-H. Chen, F.-J. Huang, and Y.-P. Fu, Phys. Rev. B **105**, 224401 (2022).